Woodwind instrument design optimization based on impedance characteristics with geometric constraints

Augustin Ernoult, Christophe Vergez, Samy Missoum, Philippe Guillemain, Michael Jousserand

Woodwind instrument design optimization based on impedance characteristics with geometric constraints

Augustin Ernoult[a,b,*], Christophe Vergez[a], Samy Missoum[c], Philippe Guillemain[a], Michael Jousserand[d]

[a] *Aix Marseille Univ., CNRS, Centrale Marseille, LMA UMR 7031, Marseille, France*
[b] *Magique 3D team, Inria Bordeaux Sud Ouest, 200 avenue de la vieille tour, 33405 Talence Cedex, France*
[c] *Aerospace and Mechanical Engineering Department, University of Arizona, Tucson, Arizona, 85721, USA*
[d] *Buffet Crampon, 5 rue Maurice Berteaux, 78711 Mantes-La-Ville, France*

Abstract

Computational optimization algorithms coupled with acoustic models of wind instruments provide instrument makers an opportunity to explore new designs. Specifically, they give the possibility to automatically find geometries exhibiting desired resonance characteristics. In this paper, the design optimization of woodwind instruments with complex geometrical features (e.g., non-cylindrical bore profile and side holes with various radii and chimney heights) is investigated. Optimal geometric characteristics are searched to obtain specific target frequencies or amplitude characteristics. However, woodwind instruments exhibit complex input impedance whose features might change drastically for a small variation of the geometry, thus hampering gradient-based optimization. For this reason, this paper introduces new formulations of the impedance characteristics (resonance frequencies and amplitudes). The approach is applied to an illustrative instrument subjected to geometric constraints similar to the ones encountered by manufacturers (a key-less pentatonic clarinet with two-registers). Three optimization problems are considered, demonstrating a strategy to simultaneously adjust several impedance characteristics on all the fingerings.

Keywords: Musical acoustics, Woodwind instruments, Bore profile optimization, Impedance characteristics, Musical instrument design

1. Introduction

Wind instrument makers typically rely on their empirical knowledge to improve an existing instrument or to design a new model. For instance, their experience of existing instruments help them select suitable inner geometries of the instrument. Once a new prototype has been manufactured, maybe with the help of new tools (e.g., reamers, mandrels), the instrument can then be evaluated by musicians. Modifications can then be carried out based on the manufacturers experience to mitigate any potential problem. This procedure is repeated until a satisfactory instrument, which is typically a compromise between different desired features (e.g., tuning of all notes), is reached. This is an iterative process, which often requires building many prototypes and is therefore costly and time consuming. In addition, the empirical design and manufacturing process leads to solutions and geometries that are close to existing ones. For this reason, it is important to provide manufacturers and the musical acoustics community strategies to facilitate and expand the design of new wind instruments.

From a physical point of view, a wind instrument can be described as a nonlinear sound source coupled with a resonator. The resonator is generally reduced to its linear response represented by its input impedance defined in the frequency domain as the ratio between the acoustic pressure and the volume flow at the entrance of the instrument. The knowledge of the input impedance and more particularly of its

*Corresponding author
Email address: augustin.ernoult@inria.fr (Augustin Ernoult)

modal characteristics (frequencies, peak amplitudes and quality-factors) allows one to explain and predict a large range of behaviors exhibited by wind instruments [1]. Many well established solutions are available to compute the input impedance from the geometry of the resonator with a good accuracy for the majority of resonator geometries [1, 2, 3, 4, 5, 6, 7, 8]. The input impedance may therefore be useful to obtain resonance frequencies and peak amplitudes of an instrument design without the need to build the corresponding prototype. Such an approach was proposed by the platform PAFI [9, 10]. If the target (desired) characteristics of the input impedance are known, it is also possible to use optimization techniques to solve the inverse problem and iteratively converge towards an optimal resonator geometry with desired impedance characteristics. The ability of optimization algorithms to find solution in a large design space can lead to unexpected configurations, sometimes markedly different from existing instruments.

However, the design optimization of wind instruments can be hampered by several challenges. Due to their nonlinear nature, wind instruments can exhibit drastic changes in behaviors for small variations of their design parameters (e.g., leading to different regimes of oscillation). This high sensitivity of the acoustic behavior can be accounted through a complete modeling of the instrument and digital sound synthesis. Another difficulty stems from the dimensionality of the optimization problem. For instance, in Tournemenne et al. [11], an optimization was carried out based on a target playing frequency. The optimization algorithm, which was tailored to tackle the complex dynamic behavior of the self-oscillating system, was used with 10 variables at most. However, considering complex bore and holes geometries would require many more design variables, which is the main reason why most authors work on optimization methods based on the input impedance only. Kausel [12] ran an optimization with 100 variables on a brass instrument using a zero-order optimization approach. Gradient-based optimization methods with analytical gradients were also used (Noreland [13]) for the optimization of conical pipes with a up to 400 variables defining the brass bore profile. Strategies to reduce the number of design variables can also be found in the literature. For instance, Braden [14] used a parameterization of the geometry of a brass bell through a few Bessel horns. The choice of the impedance characteristics to optimize is also crucial in the optimization process. For brass instrument, cost functions based on the tuning of the resonance frequencies are convenient [13, 14]. This appears not sufficient for woodwind instruments optimization which have a register hole [15]. In the latter case, the magnitude of the peaks of the input impedance must be considered as well, as proposed by Guilloteau [16]. It is therefore necessary to simultaneously adjust different types of input impedance characteristics.

This article deals with the optimization of some geometrical features of a woodwind instrument, including holes positions and dimensions. Different objective functions are considered, relying exclusively on modal characteristics of the input impedance for all fingerings. The instrument is modeled as a lattice of branched tubes (holes). As a consequence, secondary resonances, cutoff frequencies due to the holes [17], and input impedances of increased complexity can occur. Specifically, an optimization based on a typical mode tracking procedure would be hindered. This type of difficulty had not been identified in previous papers on woodwind instruments design optimization [15, 18]. This may be due to the focus which was put on the so-called logical clarinets, which have regular geometries for which the shape of the input impedance is not challenging, at least until high frequencies. To address the issue originating from the proposed complex geometry, a new phase-based description of the resonances is used in the optimization process. This new formulation enable the construction of cost functions enforcing specific target resonance frequencies in addition to target amplitude properties.

The input impedance model is presented in Section 2. The proposed new formulations of the resonance characteristics are explained in Section 3. Section 4 presents the general optimization problem formulation and the algorithm used. Finally, the proposed approach is demonstrated on the design optimization of an illustrative key-less pentatonic clarinet with two-registers in Section 5. Three optimization problems are considered involving target resonance frequencies or peak amplitude ratios as well as geometric constraints. A reference configuration is obtained through an optimization of the clarinet based on a low-frequency model. The influence of the initial design and the robustness of the algorithm are discussed in Section 6

2. Input impedance model of a woodwind instrument

Consider a generic woodwind instrument as depicted in Figure 1. The instrument consists the assembly of N_{elem} elements which can be conical or cylindrical segments with or without side holes. All these elements are described with four geometric parameters (Fig. 1): the distance to the precedent element $l(n)$, the main pipe radius $r_{pipe}(n)$ and, if their is a hole, the hole radius $r_{hole}(n)$ and the chimney height $h_{hole}(n)$. Note that in real-world instruments, the geometric properties of the elements (i.e., radii, chimney heights, and segments lengths) must satisfy specific geometric constraints, which is an primal aspect of this research.

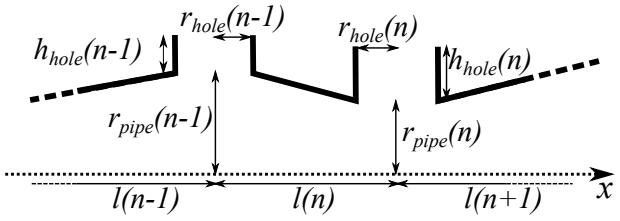

Figure 1: Sketch of the resonator of a generic woodwind instrument defined as a chain of basic elements (e.g., conical/cylindrical segments and holes)

In order to characterize the acoustical properties an optimize the design of the instrument, the input impedance Z is used:

$$Z = \frac{A_{tot} Z_{rad} + B_{tot}}{C_{tot} Z_{rad} + D_{tot}} \tag{1}$$

where Z_{rad} is the radiation impedance at the end of the pipe. $A_{tot}, B_{tot}, C_{tot}, D_{tot}$ are the coefficients of the transfer matrix M_{tot} between the input and the output of the resonator. The total transfer matrix is computed by the transfer matrix method as the product of N_{elem} elementary transfer matrices M_i [1]:

$$M_{tot} = \prod_{i=1}^{N_{elem}} M_i. \tag{2}$$

An element is defined as either a conical pipe or a side hole (T-joint). The hole transfer matrices are based on a model proposed by Lefebvre *et al.* [19]. The model accounts for the presence of chimneys and implements various length corrections. Thermoviscous losses in the chimneys are also considered to correctly estimate the magnitude of the resonances. This is especially true for a long and thin chimney, which is generally the case for the register hole. The model proposed in [19] also includes a frequency dependence for the internal length correction. However this dependence is neglected as it does not significantly affect the lower modes, which are the focus of this article, while markedly increasing the computational time.

The conical pipes (or cylinders) are modeled based on the formulation which accounts for thermoviscous losses proposed by Hélie [6]. The cone transfer matrix is

$$M_{cone} = \begin{pmatrix} A_{cone} & B_{cone} \\ C_{cone} & D_{cone} \end{pmatrix}, \tag{3}$$

where

$$\begin{cases} A_{cone} = & \frac{r_2}{r_1}\cosh(\Gamma L) - \frac{(r_2 - r_1)}{r_1 \Gamma L}\sinh(\Gamma L) \\ B_{cone} = & \frac{\rho c}{\pi r_1 r_2}\sinh(\Gamma L) \\ C_{cone} = & (A_{cone} D_{cone} - 1)/B_{cone} \\ D_{cone} = & \frac{r_2}{r_1}\cosh(\Gamma L) + \frac{(r_2 - r_1)}{r_2 \Gamma L}\sinh(\Gamma L) \end{cases}, \tag{4}$$

where r_1 and r_2 ($r_2 \geq r_1$) are the cone radii, L, the curvi-linear length (wall length), ρ and c are the air density and the sound velocity respectively. The complex wavenumber Γ which accounts visco-thermal

losses, is defined as:

$$\begin{cases} \Gamma^2 & = (jk)^2 + 2\varepsilon k^{3/2} \\ \varepsilon & = \varepsilon^* \sqrt{1 - (\frac{r_2 - r_1}{L})^2} \dfrac{\log(1 + \frac{r_2 - r_1}{r_1})}{r_2 - r_1} \end{cases} \tag{5}$$

k is the wavenumber and ε^* is a coefficient related to the temperature [6]. Note that the ratio in the form $\log(1+x)/x$ has a finite limit at $x = 0$ (i.e., $r_2 = r_1$) must be treated with special attention for elements transitioning from a cone to a cylinder or conversely.

In this work, the radiation impedance of both the main pipe and the side holes are modeled by the unflanged pipe radiation impedance approximated by a *non-causal* formulation (Silva *et al.* [20]):

$$Z_{rad} = -j \tan\left(k\mathscr{L}_{rad}(k,r) - j\frac{1}{2} \ln|\mathscr{R}_{rad}(k,r)| \right), \tag{6}$$

where k is the wave number and $\mathscr{L}_{rad}(k,r)$ and $\mathscr{R}_{rad}(k,r)$ are rational fractions depending on k and the radius r of the radiating opening.

3. Resonance characteristics

This article aims to optimize a woodwind instrument based on the peak frequencies and amplitudes of its input impedance. Specifically, resonance frequencies should match specific target values. As for the peak amplitudes, the proposed optimization enforces amplitude ratios between peaks. These requirements are obtained by the formulation of residuals related to resonances frequencies or peak amplitude. These residuals, and this is an essential aspect of this work, are constructed by taking into account the woodwind instrument specificities to assure their continuity and smoothness in the design domain.

3.1. Resonance frequencies

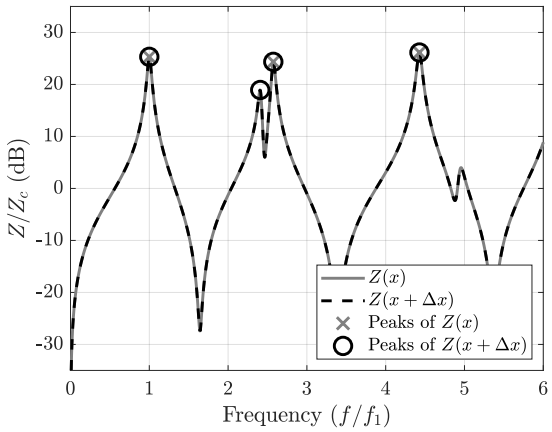

Figure 2: Example of peak detection issue (minimal prominence: 12 dB): a supplementary peak is detected for a small variation of the geometry ($\Delta x_{12} = 10^{-10}$ and $\Delta x_i = 0$ for $i \neq 12$).

Resonance frequencies are generally estimated with a global modal analysis [21] or a peak detection approach [15]. However, woodwind instrument toneholes, which can be seen as multiple parallel tubes, impose local and global cutoff frequencies [17]. As a consequence, a small variation of the geometry can lead to the appearance or disappearance of impedance peaks. The frequency of the n^{th} resonance can therefore jump from one value to another for a small variation of the geometric parameters. Figure 2 provides an example of such a problem for the second resonance.

In the context of optimization, objective functions based on the tracking of specific resonances can lead to non-smooth problems. Discontinuinuities appear for peak detection approaches based on the search of zero crossing of the imaginary part of the impedance or of the derivative of the modulus.

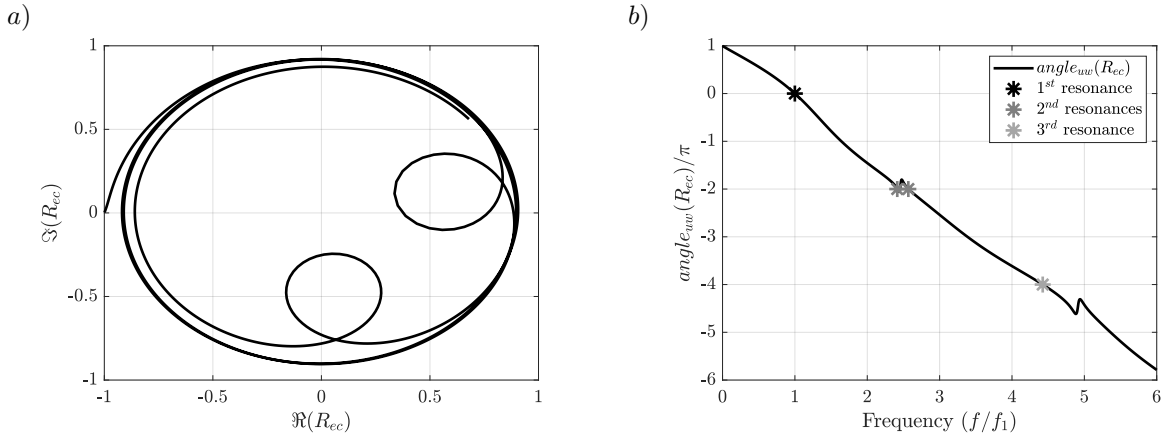

Figure 3: The reflection function R_{ec} (a) corresponding to the impedance of Fig. 2 and its unwrapped phase (b).

In order to mitigate the consequences of the non-smoothness due to traditional peak detection approach, a new approach is proposed in which the identification of the n^{th} resonance frequency is not based on the explicit enumeration of the peaks. Instead, resonances are identified based on the unwrapped phase angle of the reflection function:

$$R_{ec} = \frac{Z_{in} - Z_c}{Z_{in} + Z_c}, \tag{7}$$

which can be seen as the transfer function between incident and reflected waves observed at the input of the resonator. If the resonator induces a time delay between incident and reflected waves constant for all frequencies (a cylinder with perfect radiation condition), the phase angle of this reflection function decreases linearly with the frequency. For a real resonator the time delay can depend slightly on the frequency but the phase angle of the reflection function stays globally decreasing. Furthermore, by assuming that the resonance frequencies are defined as the poles of the input impedance, they correspond frequencies at which the phase angle is a multiple of 2π (Fig.3.b). The frequency f_n of the n^{th} resonance is therefore identified through:

$$\text{angle}_{uw}\left(R_{ec}(f_n)\right) = -2\pi(n-1), \tag{8}$$

with $\text{angle}_{uw}\left(R_{ec}\right)$ the unwrapped angle of the reflection function. This definition allows the identification of the n^{th} resonance without enumerating the lower ones.

Sometimes, due to the cutoff frequency, double resonance frequencies can appear. Figure 2 shows a case where the second resonance is double: two frequencies verify $\text{angle}_{uw}\left(R_{ec}(f_n)\right) = -2\pi$. These double resonances correspond to a loop on the complex representation of the reflection function which crosses once more the real axis (Fig.3.a). It induces fluctuations on the decrease of the angle (Fig.3.b). This double definition can be problematic if the aim is to determine an unique second resonance frequency. It is typically the case if the cost functions of the optimization problem uses the residual between the estimated resonance frequency f_n and its target $f_n^{\odot}$ [15]: $(f_n - f_n^{\odot})$. However, in this study, this difficulty is avoided by using an opposite approach taking advantage on the resonance definition of Eq. 8. Here, only the phase at the target resonance frequencies are observed. The cost functions quantify the deviation between the unwrapped phase of the reflection function at these frequencies and their target value. It is done through the residual: $\text{angle}_{uw}\left(R_{ec}(f_n^{\odot})\right) + 2\pi(n-1)$

3.1.1. Computation of the unwrapped angle

The definition of the reflection function assure its differentiability if Z_{in} is differentiable. But the traditional definition of the unwrapped angle induces some irregularities due to a definition modulo 2π. The avoid this problem another expression is used to compute the unwrapped angle. Starting from the definition of the phase angle $\varphi = \arctan\left(\Im(R_{ec})/\Re(R_{ec})\right)$, its variation is:

$$\frac{d\varphi}{df} = \frac{1}{|R_{ec}|^2}\left(\Re(R_{ec})\frac{d\Im(R_{ec})}{df} - \Im(R_{ec})\frac{d\Re(R_{ec})}{df}\right).$$

The unwrapped angle is obtained by integrating this expression from 0:

$$\begin{aligned}\text{angle}_{uw}\left(R_{ec}(f)\right) &= \int_0^f \frac{\Re(R_{ec})}{|R_{ec}|^2}\frac{d\Im(R_{ec})}{df}df - \int_0^f \frac{\Im(R_{ec})}{|R_{ec}|^2}\frac{d\Re(R_{ec})}{df}df, \\ &= \int_0^f cos(\varphi)\frac{d(sin(\varphi))}{df}df - \int_0^f sin(\varphi)\frac{d(cos(\varphi))}{df}df. \end{aligned} \quad (9)$$

It can be seen as the surface covered in the complex plane by a function having the same angle than R_{ec} but a modulus equal to the unity for every frequencies. This expression avoids discontinuities due to the definition modulo 2π of φ and seems differentiable. However, a problem occurs when a loop corresponding to a secondary resonances crosses the origin of the complex plane. If a small change of the geometry implies a new crossing of the origin, it will abruptly add -2π to the higher frequencies. The value of this angle at one given frequency shows therefore a discontinuity when a loop at lowest frequency crosses the origin. If it occurs before a target frequency, it induces a discontinuity of the residual obtained from Eq.(8). It is necessary to regularize this definition.

The discontinuity comes from the angle definition Eq.(9). The reflection coefficient being differentiable, its integration along the frequency axis is too. For the reflection coefficient, when a loop crosses the origin, the irregularity of the angle is compensated by the modulus which equals zero. The discontinuity of the angle comes from the fact that the modulus is set to one for every frequency in Equation (9). A way to regularize the angle is to restore a modulus $\tilde{R}$ which equals zeros when the modulus of the reflection coefficient is zero and one when is big enough:

$$\begin{cases} \tilde{R} = 0.5 + 0.5\cos\left(\pi\dfrac{|R_{ec}| - T_R}{T_R}\right) & \text{if } |R_{ec}| \leq T_R \\ \tilde{R} = 1 & \text{otherwise} \end{cases}, \quad (10)$$

with T_R an arbitrary threshold. The regularized unwrapped angle ϕ is therefore compute as

$$\text{angle}_{uw}\left(R_{ec}\right)(f) \approx \phi(f) = \int_0^f \tilde{R}cos(\varphi)\frac{d(\tilde{R}sin(\varphi))}{df}df - \int_0^f \tilde{R}sin(\varphi)\frac{d(\tilde{R}cos(\varphi))}{df}df. \quad (11)$$

If the loops of the reflection function are perfectly symmetric in the complex plane, this definition does not affect the value of the unwrapped angle for other frequencies whatever is the threshold T_R. However, due to thermoviscous losses, the loop are slightly asymmetric (Fig.3, *a*) and the regularization induces small bias to estimated angle of higher frequency. The threshold T_R must be chosen small enough to limit this bias, but not too small to keep the researched regularization. It is fixed here, after several test, at $T_R = 0.25$.

3.2. Resonance amplitudes

To evaluate the amplitude of the n^{th} resonance it is first necessary to localize the corresponding peak which can be done with the phase ϕ of the reflection function. Even in the case where the impedance peak

does not exactly correspond to the impedance pole, the peak is assumed to be in the domain $\mathscr{A}_n$ bounded as follows:

$$|\phi(f) - 2\pi(n-1)| \leq \phi_0, \quad \forall f \in \mathscr{A}_n, \tag{12}$$

with $\phi_0 \leq \pi$. This frequency domain is possibly discontinuous due to the fluctuation of the unwrapped angle(Sec.3.1). The magnitude of the n^{th} peak is the maximum of the impedance modulus over this domain. However, the maximum is not a differentiable function. It is therefore replaced by the p-norm:

$$a_n = \left[\sum_{f \in \widetilde{\mathscr{A}_n}} (\gamma_n(f)|Z(f)|)^p \right]^{1/p} \tag{13}$$

with p a positive number large enough to approach the maximal function but not too large to keep the differentiability (hereafter $p = 8$), $\widetilde{\mathscr{A}_n}$ an extension of the domain $\mathscr{A}_n$ and $\gamma_n(f)$ a ponderation function defined as:

$$|\phi(f) - 2\pi(n-1)| \leq \phi_1, \quad \forall f \in \widetilde{\mathscr{A}_n} \tag{14}$$

$$\begin{cases} \gamma_n(f) = \frac{1}{2}\left(1 + \cos(\frac{\phi(f)-\phi_0}{\phi_1-\phi_0}\pi)\right), & \text{if } \phi_0 \leq \phi(f) \leq \phi_1 \\ \gamma_n(f) = 1 & \text{if } \phi(f) \leq \phi_0 \\ \gamma_n(f) = 0 & \text{if } \phi(f) \geq \phi_1 \end{cases} \tag{15}$$

to avoid discontinuities due to numerical issues at the boundary of $\mathscr{A}_n$. Here, $\phi_0 = \pi/4$ and $\phi_1 = 0.9\pi$.

4. Optimization problem

4.1. General formulation

When playing a woodwind instrument several fingerings are used. Each fingering is associated with a specific input impedance computed by modifying the transfer matrices of the closed tone holes (Sec. 2). In this study, for each fingering, we consider adjusting the resonance frequencies as well as the ratio of the magnitude of the corresponding peaks as part of the optimization process.

Based on the discussion of Section 3.1, the n^{th} resonance frequency of the i^{th} fingering is evaluated by the cost function

$$\Phi_{n,i}(\mathbf{x}) = \left(\frac{\phi(f^{\odot}_{n,i})}{2\pi} + (n-1) \right)^2, \tag{16}$$

where $f^{\odot}_{n,i}$ is the target frequency of the n^{th} resonance of the i^{th} fingering.

Similarly, to enforce the ratio between two peak amplitudes $a_{2,i}$ and $a_{1,i}$, the residual A_i reads:

$$A_i(\mathbf{x}) = \left(\frac{a_{2,i}/a_{1,i} - r_i^{\odot}}{r_i^{\odot}} \right)^2 \tag{17}$$

with $r_i^{\odot}$ the target ratio for the i^{th} fingering. The general formulation of the optimization problem we wish to solve is:

$$\begin{aligned} \min_{\mathbf{x}} \quad & P(\mathbf{x}) \\ s.t. \quad & h_{geo}(\mathbf{x}) \leq 0 \\ & g(\mathbf{x}) \leq 0 \\ & \mathbf{x}_{min} \leq \mathbf{x} \leq \mathbf{x}_{max} \end{aligned} \tag{18}$$

where P and g are objective function and constraints involving a combination of Φ_i and A_i. h_{geo} are geometric constraints related to the spatial positioning and dimensions of the holes. The vector of design variables is scaled so that and $\mathbf{x}_{min} = 0$ and $\mathbf{x}_{max} = 1$.

4.2. Numerical aspects

The phase computation $\phi(f)$ in Equation (11) requires a differentiation and an integration. While the differentiation is computed through finite differences, the integration is carried out through the rectangle rule. Both operations are sensitive to the frequency step. A constant step of 1 Hz over the frequency range appears to be a good compromise between accuracy and computational time. For the cost function Φ it is necessary to evaluate the corresponding phase at the prescribed target frequencies (Eq.16). To avoid an interpolation, the target frequencies are added to the set of frequencies used for the impedance computation.

In this study, the optimizations are carried out using sequential quadratic programming (SQP). This is a well-known gradient-based algorithm for nonlinear optimization problems ([22], Chap.18). It is implemented in MATLAB through the fmincon function. SQP solves a nonlinear optimization problem through a succession of convex subproblem based on a quadratic approximation of the objective function and a linearization of the constraints. The Hessian is not exactly computed but it is approximated and iteratively updated using the gradient and the function values of the objective function. As any gradient-based method, SQP is a local optimization method and might converge to a local minimum in the neighborhood of the initialization, which must therefore be chosen carefully. At convergence, the Karush-Kuhn-Tucker (KKT) optimality conditions must be satisfied ([22], Chap.12). The KKT conditions are first-order and are therefore only necessary conditions. In this study, the tolerance for the first order optimality indicator is set to 10^{-6} while the tolerances on a relative change of iterate and objective function are set to 10^{-10} and 10^{-6} respectively. The gradients are estimated by centered finite differences with a step of 10^{-7}. This value was found after a systematic numerical investigation and showed to provide a good compromise between accuracy of the finite differences and numerical noise.

5. Results for an illustrative instrument

The instrument treated in this study is a fictive instrument including constraints which could correspond to ergonomic constraints for a real instruments. The aim is to have a two-register clarinet-like instrument (a second register one octave and a fifth higher than the first register) which can be played without keypads and without forked-fingerings (logical instrument [15]) on a range similar to a traditional clarinet (from D_3 to $G_4\sharp$ for the sounding pitch of a $B\flat$ clarinet). Following this short design specification, the first register range of one octave and a half must be covered by, at most, nine tone holes (plus one register hole), which implies at most five notes per octave. The pentatonic is therefore chosen: a C-major pentatonic scale from D for the first register, giving a G-major pentatonic scale for the second register (Table 3). The range of this instrument is similar to the one of a traditional $B\flat$ clarinet (D_3 to A_4 for the first register).

After having defined the design variables (Sec. 5.1) , the geometric constraints (Sec. 5.2) and the targeted impedance characteristics (Sec. 5.3), the method used to obtain the initial geometry is described (Sec. 5.4). Three illustrative optimization problems are then presented on this pentatonic clarinet.

1. the tuning of the first register only (Sec. 5.5)
2. the tuning of the two registers (Sec. 5.6)
3. the ratio of magnitudes of the first two resonance pics are optimized under the tuning constraints of the two registers (Sec. 5.7)

5.1. The design variables

The geometry of this instrument must be composed of at least eleven elements: the entrance of the pipe ($n = 1$), one register hole ($n = 2$), eight tone holes ($n \in [3, 10]$) and the final termination ($n = 11$). The main pipe radius at the entrance is fixed to $r_{pipe}(1) = 7.45$ mm which is the typical output radius of a $B\flat$ clarinet mouthpiece.

The design variables are (Fig. 1):

- for each hole: the hole radius $r_{pipe}(n)$, the chimney height $h_{hole}(n)$, the distance to the precedent hole $l(n)$, and the main pipe radius at the position of the hole $r_{pipe}(n)$
- the main pipe radius at the final termination $r_{pipe}(11)$ and its distance to the last hole $l(11)$

giving $N_x = 38$ variables of design summarized in Table 1.

Elements	Type	Design variables
$n = 1$	entrance	0: all fixed
$n = 2$	register hole	4: $r_{pipe}, l, r_{hole}, h_{hole}$
$n \in [\![3, 10]\!]$	tone holes	4: $r_{pipe}, l, r_{hole}, h_{hole}$
$n = 11$	final term.	2 : r_{pipe} and l

Table 1: Geometry elements

5.2. Variable ranges and geometric constraints

From a manufacturing point of view, there are three types of geometric constraints. Some are physical: a side hole can't be wider than the main pipe; some are linked to the manufacturing process: if the main pipe is drilled with a reamer, only monotonic conicity can be built; and some are ergonomic: if the holes are blocked directly by the fingers, the hole radius and the distance between them are limited by the dimensions of the human hand. Mathematically they are organized in this study according to three types: restricted authorized range, linear equality between parameters and linear inequalities.

Param.	Elements	Min.	Max.
r_{pipe}	$\forall n$	5 mm	15 mm
h_{hole}	$\forall n$	3 mm	20 mm
r_{hole}	$n = 2$	1 mm	7.5 mm
r_{hole}	$n \in \{3, 4, 5, 7, 8, 9\}$	2 mm	6 mm
r_{hole}	$n \in \{6, 10\}$	2 mm	5 mm
l	$n \in \{2, 3, 11\}$	1 mm	150 mm
l	$n \in \{4, 5, 6, 8, 9, 10\}$	10 mm	30 mm
l	$n = 7$	10 mm	150 mm

Table 2: Boundaries of the variables of design

The authorized range of the different variables are summarized in Table 2. The range of the main pipe radius r_{pipe} is chosen to prevent excessively steep flares or strangles. The range of the hole radii are fixed to be smaller than the dimension of the fingers (larger for the thumb ($n = 2$) and thinner for the little fingers ($n \in \{6, 10\}$)), but wide enough to avoid non-linear effects which could be important in small holes. Excepting the thumb, the distance $l(n)$ between successive holes is imposed to be longer than 10mm and shorter than 30 mm for fingerings of the same hand. The other distances can vary freely, which is why a large upper bound (150 mm) was chosen. This bound is never reached across all the optimizations presented in this work. The $N_x = 38$ design variables are grouped in the normalized vector $\mathbf{x}$, defined such that each component x_i equals 0 when the variable reaches its lower boundary and 1 at its upper boundary.

Linear relations between parameters are added to these boundaries. For each hole, the hole radius must be smaller than the main pipe radius with a margin of 1mm:

$$r_{hole}(n) - r_{pipe}(n) \leq -1\text{mm} \qquad \text{for } n \in [\![2, 10]\!]. \tag{19}$$

The relation

$$r_{hole}(n-1) + r_{hole}(n) - l(n) \leq -4\text{mm} \qquad \text{for } n \in [\![4, 10]\!]. \tag{20}$$

avoids the overlapping of tone-holes and assures that the tone holes are covered correctly, by guaranteeing a minimal distance of 4mm between tone holes boundaries, excluding the register hole. In actual clarinets, the register hole chimney sticks out into the main pipe. Therefore, the height of the register hole is limited by the bore diameter:

$$h_{hole}(2) - 2r_{pipe}(2) \leq -1\text{mm}, \tag{21}$$

here again a margin of 1mm is imposed. Finally, due the conical sections, a condition on the chimney height must be added to ensure that the top of the chimneys emerge from the main pipe. The following relations are imposed for all the holes ($n \in [\![2, 10]\!]$) (see Fig.1)

$$\begin{cases} h_{hole}(n) \geq r_{pipe}(n-1) - r_{pipe}(n) \\ h_{hole}(n) \geq r_{pipe}(n+1) - r_{pipe}(n) \end{cases}, \tag{22}$$

which imposes that the top of a chimney is more distant to the main axis than the main pipe at the surrounding holes. Here, there is no manufacturing constraints on the conicity. This can be justified by the use of an additive manufacturing. In this study, to simplify the equations, all the linear relations between the variables are grouped under the nomenclature $h_{geo}(\mathbf{x}) \leq 0$.

5.3. Target values

The aim of this study is to present the process. For reasons of confidentiality, the target value for the different acoustic characteristics are chosen arbitrarily. The aim is not to build a real instrument which plays in tune, but to have a resonator with the desired acoustic characteristics under geometric constraints.

Fingering index i	1	2	3	4	5	6	7	8	9
Notes	D_3	E_3	G_3	A_3	C_4	D_4	E_4	G_4	A_4
Tone holes open	0	1	2	3	4	5	6	7	8
Register hole	•	•	•	•	•	•	•	•	•
$f^{\odot}_{1,i}$ (Hz)	147	165	196	220	262	294	330	392	440
$f^{\odot}_{2,i}$ (Hz)	/	/	/	/	/	/	/	/	/
$r^{\odot}_i$	0.5	0.5	0.5	0.5	0.5	0.5	0.5	0.5	0.5

a) First register

Fingering index i	10	11	12	13	14	15	16	17	18
Notes	A_4	B_4	D_5	E_5	G_5	A_5	B_5	D_6	E_6
Tone holes open	0	1	2	3	4	5	6	7	8
Register hole	○	○	○	○	○	○	○	○	○
$f^{\odot}_{1,i}$ (Hz)	/	/	/	/	/	/	/	/	/
$f^{\odot}_{2,i}$ (Hz)	440	494	587	659	784	880	988	1175	1319
$r^{\odot}_i$	2	1.89	1.74	1.63	1.47	1.37	1.26	1.11	1

b) Second register

Table 3: Target scale of the pentatonic clarinet: first (Tab. 3 *a*) and second (Tab. 3 *b*) register, with the number of tone holes open (register hole excluded), the opening of the register hole (• : closed, ○ : open), the target values for the two first resonance frequencies $f^{\odot}_{1,i}$ and $f^{\odot}_{2,i}$ (/ : no target value) and for the ratio of their magnitude $r^{\odot}_i$.

For the fingerings of the first register (register hole closed), the target first resonance frequencies $f^{\odot}_{1,i}$ are the frequencies of the equal temperament in reference to $A_4 = 440$ Hz. For the fingerings of the second register (register hole open), it is the value of the second resonance frequencies $f^{\odot}_{2,i}$ which are targeted to the frequencies of the equal temperament and the first resonance frequencies are ignored. The aim of a register hole being to decrease the amplitude of the first resonance peak, a third parameter is observed: the ratio of the magnitude of the two first resonances a_2/a_1, as suggested by Guilloteau [18, 16]. The target value of this ratio is fixed to $r^{\odot}_i = 0.5$ on the first register ($i \in [1, 9]$), which is a typical value for a cylinder. For the second register, the playing on the second resonance, is facilitated if this ratio is above 1. Following the studies of Guilloteau [18, 16] a linear decrease of r_i with the pitch is observed experimentally for one register hole. The arbitrary choice of a ratio from 2 at the bottom of the second register to 1 at its top is made. All these target values are summarized in Table 3.

5.4. Low frequency approximation as a 1st-order design

As proposed by Noreland [15], it is possible to estimate analytically a geometry by using the low frequency approximations to place the holes. This geometry can be used to initialize the algorithms. In low frequency approximation, all the elements can be approximated by inertance which can be interpreted as length correction from the entrance cross-section ($\pi r_{pipe}(1)^2$) leading to an effective position $P_{eff}(n)$ of each hole including:

- the effective length of the tone hole, including: the chimney height (h_{hole}), the matching volume, the "inner length" correction and the radiation length corrections [19],
- the length correction due to the downstream part of the instrument [1, Chap.7.7.5.3, p.375]
- the length correction induced by the volume added by the upstream closed chimneys [23].

For a given fingering, the effective position of the first open hole is fixed to the quarter of the target wavelength. This procedure leads to an unexplained offset of -20 cents for the final impedance. This offset is included into the target position leading to: $P_{eff}(n) = c/(4f_1 \times 2^{-20/1200})$, with c the sound velocity. If possible, the register hole is positioned to the third of the mean of the tone holes effective positions, with the longest chimney height and the thinner radius with respect to their authorized values, which tends to maximize its acoustic mass. To estimate analytically the geometry, only the distance l, the chimney height h_{hole} then the holes radii r_{hole} are modified. The main pipe radii are let to an arbitrary initial value, the entry radius: $r_{pipe}(n) = r_{pipe}(1) = 7.45$ mm for all n. The boundaries constraints are taken into account: the position is modified until it reaches a boundary, then the chimney height is modified and finally the hole radius. If the three boundaries are reached without having the desired effective position, the geometry is let with this defect. The modification of both downstream and upstream hole modifying the effective position of the hole, a loop is carried until the stagnation of the geometry.

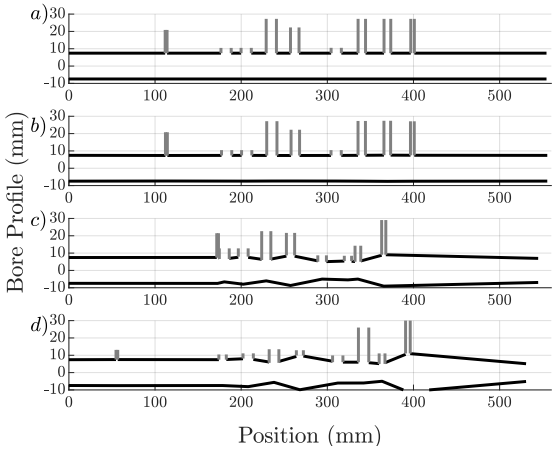

Figure 4: Comparison of geometries: (a) initial geometry (Sec. 5.4), the geometries obtained after the optimization of: (b) the first resonance frequency F (Sec. 5.5); (c) the two registers tuning $F + H$ (Sec. 5.6); (d) the ratio of magnitude of the two first resonances A under the constraint on the resonance frequencies (Sec. 5.7).

The geometry obtained for targets of Table 3.a under the constraints of Sec. 5.2 is plotted in Figure 4.a. The corresponding tuning is represented on Figure 5.a. The deviation between the first resonance frequencies and the target frequencies is within ± 10 cents except for the second fingering $F\sharp_3$. This is because all the modifiable parameters of the last hole ($n = 10$) reach their boundaries (the distance $l(10)$, the chimney height $h_{hole}(10)$, and the hole radius $r_{hole}(10)$). Due to the constraints, it should not be surprising that the process presented does not allow a satisfying tuning of the analytically designed geometry. To improve this tuning it is necessary to use an optimization algorithm.

5.5. Problem formulation 1: first register tuning

For this first optimization problem only the tuning of the first register (9 fingerings) is considered (Table 3.a). Following the discussion on the sections 3.1, 4.1 and on the definition 16, the cost function is defined as:

$$F(\mathbf{x}) = \frac{1}{9}\sum_{i=1}^{i=9} \Phi_{1,i} = \frac{1}{9}\sum_{i=1}^{i=9} \left(\frac{\phi(f_{1,i}^{\odot})}{2\pi} \right)^2 . \tag{23}$$

In this problem only the geometric constraints (authorized ranges and linear relation between the variables, Sec. 5.2) are considered. The optimization problem can be summarized as:

$$\begin{aligned} \min_{\mathbf{x}} \quad & F(\mathbf{x}) \\ \text{subject to} \quad & h_{geo}(\mathbf{x}) \leq 0 \\ & 0 \leq \mathbf{x} \leq 1 \end{aligned} \tag{24}$$

The cost function F depends only of the phase ϕ computed at the target frequencies $f_{1,i}^{\odot}$ of the first register. Only the impedance of the 9 first fingerings must be computed (Tab. 3.a). It is furthermore not necessary to compute the frequency response of the resonator at higher frequencies than the maximal target $f_{1,i}^{\odot}$. The highest interesting frequency being 440 Hz (Tab. 3.a), the frequency range is fixed to $[0.1, 480]$ Hz.

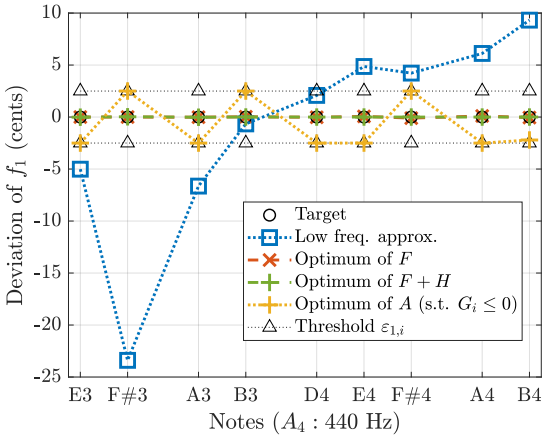

Figure 5: Deviation in cents of the first resonance frequencies from the target value for the first register (9 first fingerings). The problem with $F + H$ is presented in Sec.5.6, the threshold $\varepsilon_{1,i}$ and the problem "A s.t. G_i" are presented in Sec.5.7.

The optimization algorithm is initialized with the geometry obtained by the process presented in Sec. 5.4. The algorithm converges to a local minimum in 35 iterations computed in less than 1 minute on a standard personal computer (4 cores, 16 Go of Ram). The cost function reaches $F \approx 10^{-9}$ corresponding to deviations within 0.1 cents between the first resonance frequencies $f_{1,i}$ and their target $f_{1,i}^{\odot}$ (Fig. 5)[1]. The geometry obtained, represented in Figure 4.b, is very closed to the initial geometry (Fig. 4.a). The design variables are modified of less than 1.5% except for the last tone hole radius ($r_{hole}(10)$) which varies of about 6%.

5.6. Problem formulation 2: two registers tuning

In this second optimization problem, the tuning of the second register is included through the cost function

$$H(\mathbf{x}) = \frac{1}{9}\sum_{i=10}^{i=18} \Phi_{2,i} = \frac{1}{9}\sum_{i=10}^{i=18} \left(\frac{\phi(f_{2,i}^{\odot})}{2\pi} + 1 \right)^2 , \tag{25}$$

[1]The resonance frequencies $f_{1,i}$ are associated to the zero of the phase ϕ estimated trough a linear interpolation around the zero-crossing.

which allows to adjust the second resonance frequency of the fingerings of the second register (register hole open, Table 3.b) by following the discussion of Section 3.1 and 4.1. The simplest way to adjust simultaneously the two registers under the geometrical constraints is to treat the following optimization problem:

$$\begin{aligned} \min_{\mathbf{x}} \quad & (F(\mathbf{x}) + H(\mathbf{x})) \\ \text{s. t.} \quad & h_{geo}(\mathbf{x}) \leq 0 \\ & 0 \leq \mathbf{x} \leq 1 \end{aligned} \tag{26}$$

This time, the highest interesting frequency being 1319 Hz (Tab. 3.b), the frequency range is fixed to $[0.1, 1450]$ Hz.

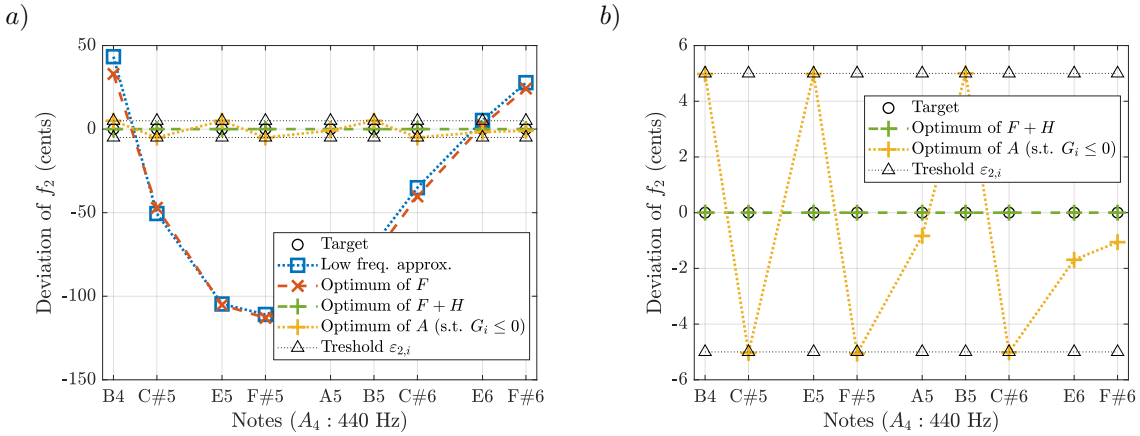

Figure 6: Deviation in cents of the second resonance frequencies from the target value for the 9 highest fingerings. *a*) for the four geometries of Fig 4; *b*) a zoom within ±5 cents with the geometries for which the second resonance frequency has been optimized. The threshold $\varepsilon_{2,i}$ and the problem "A s.t. G_i" are presented in Sec.5.7.

The optimization algorithm initialized with the geometry from Section 5.4 converges in 451 iterations (about 1 hour on a personal computer). The computation time per iteration is longer that for the first problem (Sec. 5.5) because frequency range used is wider and it is necessary to compute two times more impedances per iteration (18 fingerings against 9 for the first problem). The final cost values are $F \approx 10^{-11}$ and $H \approx 10^{-12}$, which correspond to deviations within 0.025 cents for the first register and 0.002 cents for the second one (Fig. 5, Fig. 6).

The geometry obtained is represented on Figure 4.c. Due to the addition of the cost function H, the algorithm converges here to a geometry much more different from the initialization than for the first problem (Fig. 4). However, it is noticeable that this local minimum is better both for H and F than the local optimum obtained in the first problem where only this cost function was taken into account (Sec. 5.5): here $F \approx 10^{-11}$ against $F \approx 10^{-9}$ for the first problem. This improvement is a consequence of the use of a local optimization algorithm. The initialization used (Sec.5.4) is very close to a local minimum of F, as illustrated by the similarity of the geometries (Fig.4.a and b). The addition of H in the cost function leads the algorithm to another local minimum, more different from the initialization, but better for F.

5.7. Problem formulation 3: integration of the magnitude ratio

As evoked by Guilloteau [16], to have a playable second register it is necessary to adjust the relative magnitude of the two first peaks. Following the discussion of the sections 3.2 and 4.1, the cost function

$$A(\mathbf{x}) = \frac{1}{18}\sum_{i=1}^{i=18} A_i = \frac{1}{18}\sum_{i=1}^{i=18}\left(\frac{a_{2,i}/a_{1,i} - r_i^{\odot}}{r_i^{\odot}}\right)^2, \tag{27}$$

is adapted to treat this aspect. As in Section 5.6, a simple way to minimize together F, H and A is to treat the following optimization problem:

$$\begin{aligned} \min_{\mathbf{x}} \quad & (F(\mathbf{x}) + H(\mathbf{x}) + A(\mathbf{x})) \\ \text{s. t.} \quad & h_{geo}(\mathbf{x}) \leq 0 \\ & 0 \leq \mathbf{x} \leq 1 \end{aligned} \tag{28}$$

However, the local minimum reached by starting from the initial geometry obtained with the process described in Sec. 5.4 is not satisfying. At the final state, the cost functions A and F are around 10^{-3} and $H \approx 10^{-4}$, which corresponds to a deviation higher than 100 cents for some fingerings of the first register and 40 cents for the second register. These deviations are too wide for a musical instrument. In another hand, the ratios of magnitude are within $\pm 10\%$ of their targets which is a good result whereas this aspect is not critical for musical instrument. Tests from different initial results makes appears that it is impossible to reach the target of the three cost function together. One possibility is to impose a satisfying deviation between the resonance frequencies and their target by converting the cost function F and H into non linear constraints.

In this study it seems reasonable to fix, for each fingering i, a value of the maximal deviation $\varepsilon_{n,i}$ between the n^{th} frequency resonance $f_{n,i}$ and the target $f^{\odot}_{n,i}$ for which the tuning is acceptable. This threshold is defined as:

$$\varepsilon_{n,i} \geq 1200 \log_2 \left(\frac{f_{n,i}}{f^{\odot}_{n,i}} \right), \tag{29}$$

by following the cents definition. A maximal deviation $\varepsilon_{1,i} = 2.5$ cents is chosen for the first register ($i \in [1, 9]$). For the second register, a wider deviation is authorized: $\varepsilon_{2,i} = 5$ cents for $i \in [10, 18]$. To convert the cost function F and H into inequality constraints, it is necessary to compute the corresponding authorized deviation $\zeta_{n,i}$ on the angle of the reflection coefficient ϕ at the target frequency $f^{\odot}_{n,i}$. By assuming that $f_{n,i}$ is closed to $f^{\odot}_{n,i}$, it is possible to do a Taylor development:

$$\begin{aligned} \phi(f_{n,i}) &= \phi(f^{\odot}_{n,i}) + (f_{n,i} - f^{\odot}_{n,i}) \frac{d\phi}{df}(f^{\odot}_{n,i}) \\ \phi(f^{\odot}_{n,i}) &= \phi(f_{n,i}) - f^{\odot}_{n,i} (\frac{f_{n,i}}{f^{\odot}_{n,i}} - 1) \frac{d\phi}{df}(f^{\odot}_{n,i}) \end{aligned} \tag{30}$$

The phase at the resonances being, by definition, $\phi(f_{n,i}) = -2\pi(n-1)$. The threshold $\zeta_{n,i}$ on the phase at the target frequency $\phi(f^{\odot}_{n,i})$ is therefore defined from Eq.29 by:

$$\zeta_{n,i} = (1-n) - \frac{1}{2\pi} f^{\odot}_{n,i} (2^{(\varepsilon_{n,i}/1200)} - 1) \frac{d\phi}{df}(f^{\odot}_{n,i}). \tag{31}$$

This threshold depends only on the target frequency considered and the derivative of the phase at this frequency. Numerically, this derivative is estimated from a spline interpolation around $\phi(f^{\odot}_{n,i})$. It is now possible to construct non-linear functions which are negative only when the frequency deviation between $f_{n,i}$ and $f^{\odot}_{n,i}$ is lower than the threshold:

$$G_i = \begin{cases} \Phi_{1,i} - (\zeta_{1,i})^2 & \text{for } i \in [1, 9] \\ \Phi_{2,i} - (\zeta_{2,i})^2 & \text{for } i \in [10, 18] \end{cases} \tag{32}$$

The third optimization problem is finally:

$$\begin{aligned} \min_{\mathbf{x}} \quad & A(\mathbf{x}) \\ \text{s. t.} \quad & h_{geo}(\mathbf{x}) \leq 0 \\ & 0 \leq \mathbf{x} \leq 1 \\ & G_i \leq 0 \qquad \text{for } i \in [1, 18] \end{aligned} \tag{33}$$

To be sure to correctly estimate the magnitude of the second peaks, the frequency range is extended to $[0.1, 4000]$ Hz.

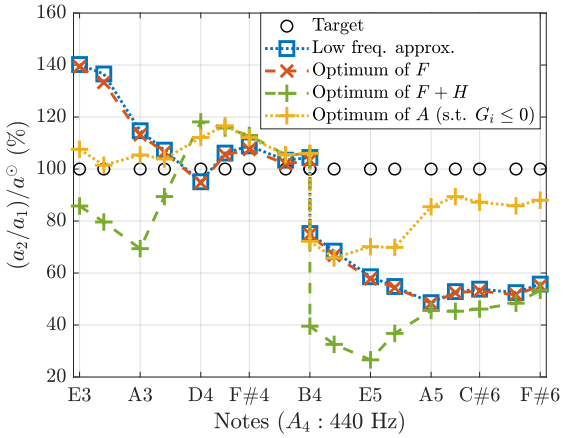

Figure 7: Ratio of magnitude of the two first frequencies resonance a_2/a_1 for each fingering, compared to the target values $a^{\odot}$.

The optimization algorithm initialized with the geometry from Section 5.4 converges in 88 iterations (about 30 min on a personal computer). The non-linear constraints G_i are well respected. The deviation between the first resonance frequencies and their targets are within ± 2.5 cents for the first register (Fig. 5) and within ± 5 cents for the second register (Fig. 6.b). The final cost value is $A \approx 2.6 \cdot 10^{-2}$. The corresponding deviations to the targets are within 20% for the most of the fingerings (Fig. 7) except for the lower part of the second register where the deviation is around 30% (from B4 to G5). By comparison with other geometries, the improvement is especially localized on the lower part of the first register and the higher part of the second one (Fig. 7).

The geometry obtained is represented on Figure 4.d. The geometry is really different from the ones obtained before: its total length is shorter, it ends with a convergent cone and the chimneys are globally shorter. A striking difference with the geometry obtained by optimizing $F + H$ (Fig. 4.c) is maybe the register hole which is here nearby the entrance with a short chimney, whereas it was as close as possible of the first tone hole with a long chimney in the previous geometry. The importance of this register hole and especially its chimney height, on the ratio of peak amplitudes was already identified by Noreland [15] and Guilloteau [16].

The high residual deviation observed between the optimum obtained and the targets illustrates well the necessary compromise, for this instrument, between the frequencies of the second register (H) and the relative magnitudes of the second peaks (A). This compromise is specific to the design problem discussed here. It is not necessary present for every woodwind instruments design. It could maybe be solved by relaxing some geometric constraints or by being less ambitious on the targets $r_i^{\odot}$ for the ratio of magnitude (a ratio of 1.5 instead of 2 for the lowest note of the second register is certainly sufficient). However the aim of this last instance is also to illustrate the possibility to deal with an acoustic compromise in an optimization problem.

6. Discussion: Influence of the initial geometry

The gradient based algorithm performing local optimization, the starting point can have a significant influence on the geometry obtained and on the convergence of the algorithm. This dependency is assessed and discussed in this section by repeating the three optimization problems 24, 26 and 33 from 19 other initial geometries. The design parameters values are taken randomly in their authorized ranges (Table 2), leading to 20 realizations of each optimization problem by including the ones already presented.

For the first problem, where only F is minimized (Sec. 5.5), the optimization process converges, in averages, in 75 iterations (around 2 min of computation). The final cost function is always below 10^{-9} with an average value around 10^{-12}. All the optima are therefore satisfying from a musical tuning point of view with a deviation between the resonance frequencies and their target within 0.1 cents, far below the human perception threshold. The optimum obtained from the initialization with low frequency approximation (Sec. 5.4) has the highest final value ($F \approx 10^{-9}$). As discussed in Section 5.6, it suggests that the local minimum the most similar to this logical initialization is not the best solution.

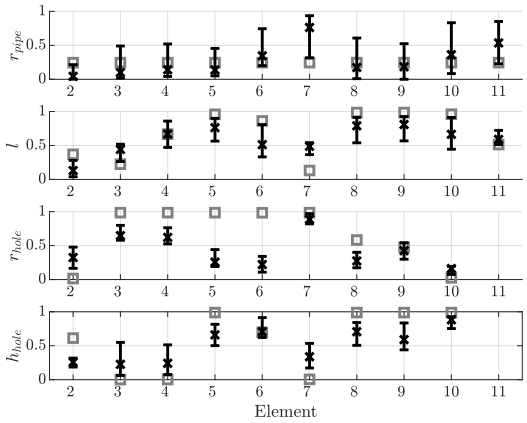

Figure 8: Boxplot representing the variability of the normalized geometric parameters of the 20 geometries obtained for the problem 1 (Equ. 24, Sec. 5.5). All the final cost values are between 10^{-14} and 10^{-9}. For each parameter, the crosses are the median and 90% of the data are within vertical bar. The gray squares correspond to the initial geometry obtained by low frequency approximation (Sec. 5.4).

The obtained geometries cover a wide variety (Fig.8). It illustrates the fact that, when only F is minimized it is an ill-posed optimization problem (several solutions are possible). This property is necessary to let the possibility to make the cost function more complex or add other constraints such as in problems 2 and 3 (Sec.5.6 and 5.7). However, it is interesting to observe that among this variability a global tendency appears. In particular the localization l of the holes and their chimney heights h_{hole} are similar to the ones of the low frequency approximation (Fig.8), whereas the main difference is concentrated on the hole radii r_{hole} (Fig.8).

For the problem 2 ($F + H$), the average number of iterations needed to reach the minimum is 486, but this number shows a wide variety among the 20 repetitions (between 142 and 2900). The final cost function values show also a wide diversity. Even if most of the optimization processes (15/20) have a good result ($F + H < 10^{-9}$, corresponding to a deviation within 0.5 cents), 4 realizations converge to a state at which $F + H > 10^{-6}$ (deviation around 10 cents) and one to $F + H \approx 10^{-3}$ for which the deviation between the resonance frequencies and their targets reaches 500 cents on some fingerings. The geometric parameters obtained for the two groups of optimums ($F+H < 10^{-9}$ and $F+H > 10^{-6}$) are represented in Figure 9. Most geometric parameters are similar for all the geometries having a good optimum ($F + H < 10^{-9}$), except for the final main pipe radius $r_{pipe}(11)$ and the position of the three last elements trough the distance $l(9)$ which can compensate each other. The two groups of geometries differ essentially by the hole radii $r_{hole}(3, 5, 6)$ and the chimney height $h_{hole}(8)$. These two groups seem to correspond to two areas of the design space. Depending on the initial state, the algorithm converges to one of these two types of geometries.

For the problem 3 (A s.t. G_i, Sec.5.7), only four realizations of the optimization process among the 20 converge correctly. The other ones reach the maximum iteration (for 4 realizations) or stop because the step length in the design space is smaller than the authorized threshold 10^{-16} (12 realizations). The four converged processes reach the minimum after, in average, 180 iterations (around 45min of computation).

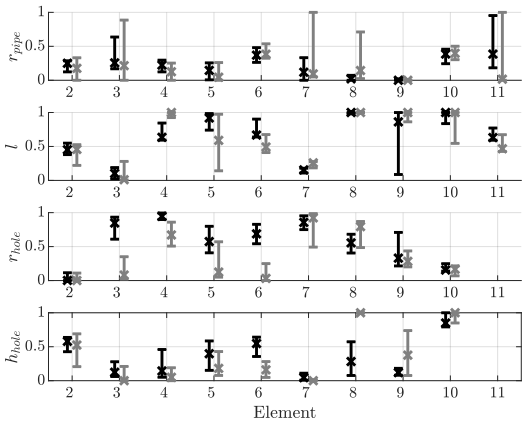

Figure 9: Boxplot representing the variability of the normalized geometric parameters of the geometries obtained for the problem 2 (Equ. 26, Sec. 5.6). For each parameter, the crosses are the median and 90% of the data are within vertical bar. The black data correspond to the 15 geometries for which $F + H < 10^{-9}$ and the gray data, the 5 geometries for which $F + H > 10^{-6}$.

Two geometries obtained are exactly identical (including the one obtained from the geometry of Section 5.4) with a final cost value $A \approx 2.6 \cdot 10^{-2}$ and the other have final cost function values around $A \approx 5 \cdot 10^{-3}$.

The non-convergence of the 16 other realizations of the optimization process can have several origins. First of all it can come from a local non-smoothness of the cost function or an error in the estimation of its gradient. Even if, in Section 3.2, the resonance amplitudes are defined by taking care of the differentiability, their numerical transcription can induce some irregularities. The numerical integration used to compute Equation (11) is sensitive to the frequency step and can induce numerical error. Further investigation is needed to improve this computation by using more accurate numerical integration techniques. This aspect can have a direct incidence on the gradient estimation which is here computed by finite difference. The knowledge of an explicit expression of the gradients could avoid this difficulty, but also allow a better estimation of the gradient, accelerate the computation and demonstrate the differentiability of the cost functions. The formulation of such an expression is a complex task which needs to be investigated in a further work.

By observing the evolution of the cost function along the design space, another difficulty appears. The representation of the cost function along the 38 dimensions of the design space being impossible, it is represented, in Figure 10, on the plane where the 9 chimney heights h_{hole} on one side, and the 10 main pipe radii r_{pipe} on the other side (Tab.1) are fixed equals and modified together. The series of oblique valleys which appear are real difficulties for optimization algorithm. The algorithm progresses slowly along one valley by jumping from one side to another. The step can become smaller and smaller and even reach the authorized threshold before a local minimum is reached. Preliminary observations suggest that the presence of these valleys is inherent in the use of peak amplitudes. There is no specific study on the relation between the geometric parameters and the resonance amplitude. Specific investigations are needed to clarify this relation and eventually find a better way to include the resonance amplitude in the optimization process. With the current definition used in this study, the initial geometry must be chosen carefully to start the optimization in the neighborhood of a local minimum.

7. Conclusion

This article describes the design optimization of a woodwind instrument with geometric constraints. In order to obtain specific impedance characteristics (peak frequencies and peak amplitude ratios), new quantities are introduced. Specifically, a new definition of the notion of resonance, based on an ad-hoc

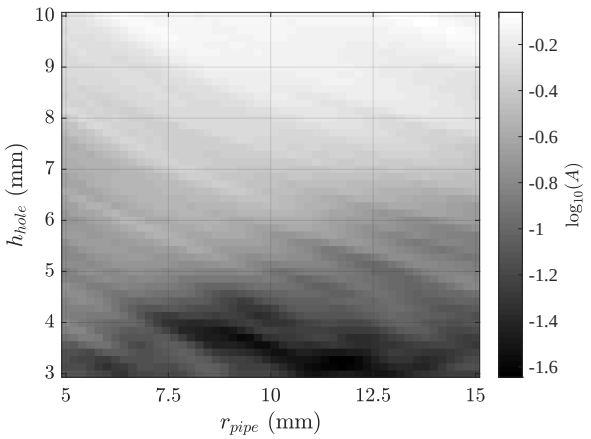

Figure 10: Evolution of the cost function A in the plane of the design space where all the pipe radii r_{pipe} and all the chimney heights h_{hole} are equal and move together, the other variables being fixed to their initial values. Several parallel valleys are visible.

unwrapping of the phase of the reflection coefficient is proposed. The purpose is to facilitate gradient-based optimization, which would otherwise be hampered by the non-smoothness of the functions. This is especially true for woodwind instruments for which the presence of side hole makes more complex the frequency response. The optimization is implemented, for high dimensional problem, on an instrument with 38 variables thus demonstrating the potential of optimization to deliver new designs.

The design of a wind instrument rarely corresponds to the minimization of a single type of quantity. For example, attempts to match resonance frequencies of the optimal solution with target frequencies cannot lead, in general, to a satisfactory musical instrument. Other characteristics might need to be taken into account. Beyond the examples chosen in this article, the inharmonicity between the first resonance frequencies for each fingering, or the radiation properties of the instrument could be considered. To treat this aspect, we have shown that it is convenient to formulate an optimization problem with a single objective function to minimize (in our case the ratio between the amplitudes of the first two peaks of the input impedance), while including new constraints on the expected result (in our case the resonance frequencies of the first two peaks are constrained around the target frequencies).

For confidentiality reasons, the examples demonstrated in this paper, in particular the choice of targets, are purely demonstrative. However, during our collaboration with our industrial partner Buffet-Crampon, other optimization results have led to the building of prototypes. The protocol for evaluating these prototypes as well as their playability as judged by the musicians are irrelevant in this article. What is worth noting, however, is that the approach proposed allows, say in one day, to launch a design by optimization, to build a prototype by 3D printing, and then to get feedback from musicians. Indeed, since the definition of a good musical instrument is not explicit, and no one yet knows how to translate it into an objective function to minimize, discussions with musicians are essential to converge towards a final solution. Therefore the design process remains iterative, as in the traditional trial-and-error approach of the instrument makers. It is therefore essential to control the time required for an iteration of "design optimization - manufacture of the prototype - evaluation by musicians". This is a strength of the proposed approach.

8. Acknowledgements

This work has been partly supported by the french Agence Nationale de la Recherche (ANR16-LCV2-0007-01 Liamfi project), in cooperation with Buffet-Crampon.

References

[1] A. Chaigne, J. Kergomard, Acoustics of Musical Instruments, Modern Acoustics and Signal Processing, Springer New York, New York, NY, 2016.

[2] R. Caussé, J. Kergomard, X. Lurton, Input impedance of brass musical instruments—Comparison between experiment and numerical models, The Journal of the Acoustical Society of America 75 (1) (1984) 241–254. doi:10.1121/1.390402.

[3] D. H. Keefe, Acoustical wave propagation in cylindrical ducts: Transmission line parameter approximations for isothermal and nonisothermal boundary conditions, The Journal of the Acoustical Society of America 75 (1) (1984) 58–62. doi:10.1121/1.390300.

[4] A. Lefebvre, Computational acoustic methods for the design of woodwind instruments, Ph.D. thesis, McGill University (2010).

[5] P. Eveno, J.-P. Dalmont, R. Caussé, J. Gilbert, Wave Propagation and Radiation in a Horn: Comparisons Between Models and Measurements, Acta Acustica united with Acustica 98 (1) (2012) 158–165. doi:10.3813/AAA.918501.

[6] T. Hélie, T. Hézard, R. Mignot, D. Matignon, One-Dimensional Acoustic Models of Horns and Comparison with Measurements, Acta Acustica united with Acustica 99 (6) (2013) 960–974. doi:10.3813/AAA.918675.

[7] J.-B. Doc, B. Lihoreau, S. Félix, V. Pagneux, Bremmer series for the multimodal sound propagation in inhomogeneous waveguides, Wave Motion 67 (2016) 55–67. doi:10.1016/j.wavemoti.2016.07.004.

[8] R. Tournemenne, J. Chabassier, A comparison of a one-dimensional finite element method and the transfer matrix method for the computation of wind music instrument impedance, Acta Acustica united with Acustica 5 (2019) 838.

[9] ITEMM, Plateforme d'aide à la facture instrumentale, http://plateforme-lutherie.com/index.html.
URL http://plateforme-lutherie.com/index.html

[10] P. Eveno, L'impédance d'entrée pour l'aide à la facture des instruments de musique à vent : mesures, modèles et lien avec les fréquences de jeu, phdthesis, Université Pierre et Marie Curie - Paris VI (Dec. 2012).

[11] R. Tournemenne, J.-F. Petiot, B. Talgorn, J. Gilbert, M. Kokkolaras, Sound simulation-based design optimization of brass wind instruments, The Journal of the Acoustical Society of America 145 (6) (2019) 3795–3804. doi:10.1121/1.5111346.

[12] W. Kausel, Optimization of Brasswind Instruments and its Application in Bore Reconstruction, Journal of New Music Research 30 (1) (2001) 69–82. doi:10.1076/jnmr.30.1.69.7117.

[13] D. Noreland, Gradient based optimisation of brass instruments, in: Stockholm Music Acoustics Conference, Stockholm \cite, 2003.

[14] A. C. P. Braden, M. J. Newton, D. M. Campbell, Trombone bore optimization based on input impedance targets, The Journal of the Acoustical Society of America 125 (4) (2009) 2404–2412. doi:10.1121/1.3087423.

[15] D. Noreland, J. Kergomard, F. Laloë, C. Vergez, P. Guillemain, A. Guilloteau, The Logical Clarinet: Numerical Optimization of the Geometry of Woodwind Instruments, Acta Acustica united with Acustica 99 (4) (2013) 615–628. doi:10.3813/AAA.918641.

[16] A. Guilloteau, P. Guillemain, J. Kergomard, M. Jousserand, On the Second Register's Playability of the Clarinet: Towards a Multicriteria Approach, in: International Symposium on Musical Acoustics, Montreal, 2017, p. 1.

[17] E. Moers, J. Kergomard, On the Cutoff Frequency of Clarinet-Like Instruments. Geometrical versus Acoustical Regularity, Acta Acustica united with Acustica 97 (6) (2011) 984–996. doi:10.3813/AAA.918480.

[18] A. Guilloteau, Conception d'une clarinette logique, Ph.D. thesis, Aix-Marseille Université, Marseille, France (Sep. 2015).

[19] A. Lefebvre, G. P. Scavone, Characterization of woodwind instrument toneholes with the finite element method, The Journal of the Acoustical Society of America 131 (4) (2012) 3153–3163.

[20] F. Silva, P. Guillemain, J. Kergomard, B. Mallaroni, A. N. Norris, Approximation formulae for the acoustic radiation impedance of a cylindrical pipe, Journal of Sound and Vibration 322 (1–2) (2009) 255–263. doi:10.1016/j.jsv.2008.11.008.

[21] P. A. Taillard, F. Silva, P. Guillemain, J. Kergomard, Modal analysis of the input impedance of wind instruments. Application to the sound synthesis of a clarinet, Applied Acoustics 141 (2018) 271–280. doi:10.1016/j.apacoust.2018.07.018.

[22] J. Nocedal, S. J. Wright, Numerical optimization, 2nd Edition, Springer series in operations research, Springer, New York, 2006, oCLC: ocm68629100.

[23] V. Debut, J. Kergomard, F. Laloë, Analysis and optimisation of the tuning of the twelfths for a clarinet resonator, Applied Acoustics 66 (4) (2005) 365–409. doi:10.1016/j.apacoust.2004.08.003.